LA-UR -85-4472

CONF-8511120

LA-UR--85-4472

DE86 004752

Los Alamos National Laboratory is operated by the University of California for the United States Department of Energy under contract W-7405-ENG-36.

TITLE: A MODEL FOR OPTICAL-LASER-INDUCED IMPULSE IN VACUO

AUTHOR(S): R. S. Dingus and S. R. Goldman

SUBMITTED TO: AIAA Laser Effects and Target Response, Menlo Park, CA, November 1985

DISCLAIMER

Los Alamos Los Alamos National Laboratory
Los Alamos, New Mexico 87545

FORM NO 836 R4

A Model for Optical-Laser-Induced Impulse in Vacuo

by

R. S. Dingus and S. R. Goldman
Los Alamos National Laboratory

Abstract

A simple model, along with its derivation, is presented for calculating the impulse from targets in a vacuum exposed to single-pulse, optical lasers. Figures demonstrate that throughout most of the range of interest, results from the model agree well with experimental data and LASNEX radiation-hydrodynamic computer code calculations. The model assumes isothermal blowoff and thus takes advantage of the insensitivity of impulse to energy distribution within the ablated mass. The density profile in the blowoff is estimated and the Saha equation is used to evaluate the degree of ionization. The laser absorption coefficient and thermal radiation opacity are evaluated as a function of position in the blowoff in order to evaluate the energy reaching the ablation surface. An overall energy balance plus an energy balance at the ablation surface are used to determine the blowoff mass and temperature. The success of the model indicates that the impulse is insensitive to detailed interactions in the vicinity of the ablation surface.

I. INTRODUCTION

The momentum per unit area induced by lasers incident on targets in a vacuum is a function the photon wavelength; the flux (intensity) as a function of time; the fluence (integral of flux over time), the angle of incidence; the beam diameter (unless it is sufficiently large); and the target's material and geometric properties. In this paper, the target is assumed to be flat, the beam incident normal to the surface, and the beam diameter sufficiently large that the blowoff is one dimensional (i.e., that gradients in the blowoff such as temperature, density, etc. only exist in the direction normal to the target surface). The region of emphasis for this paper is from the threshold for impulse up to a flux of about 10^{16} W/m^2 or to a fluence of about 10^{10} J/m^2.

Reference 1 discusses the phenomenology of optical-laser-induced impulse in vacuo and develops a model for calculating impulse in which the mass loss is allowed to be a free parameter. In this paper, another equation is developed and added to that model, thus fixing the mass loss and allowing impulse predictions to be obtained without a posteriori knowledge of the blowoff mass.

The model is most applicable in the region of moderately high flux and fluence where inverse bremsstrahlung dominates laser absorption. In this region, the results of this model agree amazingly well with both experimental data and LASNEX hydrodynamic computer-code calculations, although one-dimensional data do not exist at high fluences in this region. The model is based upon an overall energy balance plus an energy balance at the ablation surface. Although considerable attention is given to evaluating the energy transfer through the blowoff to the ablation surface, little attention (other than enthalpy considerations) is given to the complicated thermodynamics at the ablation surface. The success of the model indicates that the impulse is insensitive to detailed interactions in the vicinity of the ablation surface. This is fortunate because these interactions are not easy to assess accurately because of the large temperature, density, etc. gradients in this region.

II. IMPULSE MODEL

A. Basic Model

The model is described by a set of self-consistent equations summarized in the Appendix B. The symbols used in the equations are defined in Appendix A. Most of these equations were developed in Ref. 1. They are discussed briefly in this section; more detail can be obtained from Ref. 1. Details regarding derivation of the energy balance equations are presented in the next section. They rely upon the fact (shown in Ref. 1) that the impulse is insensitive to the distribution of kinetic energy within the blowoff mass. If the total blowoff mass and energy within are known, along with a rough approximation of the distribution of energy within the mass, then the impulse can be predicted rather accurately.

Following that lead, the model is based upon the assumption that, for any given laser pulse incident on a target, the blowoff will be isothermal with temperature T. The blowoff particles are assumed to have a Maxwell-Boltzmann distribution of velocities with an average velocity $\bar{v}$ given by

$$v = [(8/\pi)N_o kT/\bar{A}]^{1/2} , \quad \bar{A} = A/(1 + Z) . \qquad (1)$$

Further, it is assumed that the laser flux ϕ_o and the mass ablation rate $\dot{M}$ are constant during the laser pulse and that no ablation occurs after the pulse. These assumptions have been made for simplicity to allow a simple time-integrated solution to the problem. However, it appears that other temporal functions for the flux and ablation rate could also be used. Better yet, but with considerable increase in model complexity, a time-dependent solution with this basic model for an arbitrary temporal profile for the flux should be possible by solving the rate equations for the ablation rate (instead of first integrating them over time) and then stepping through time.

Using these assumptions plus the assumption that there is no interaction between the particles in the blowoff allows an equation to be derived[1] for the density ρ as a function of position z within the blowoff

$$\rho/\rho_o = \exp(-\zeta^2) , \quad \rho_o = [4/\pi][\dot{M}]/v ,$$
$$\zeta = [4/\pi][z/z_o] , \quad z_o = v\tau , \quad m/M = \mathrm{erf}(\zeta) ,$$
$$m = m(z) = \int_o^z \rho(z')dz' , \quad M = m(\infty) ,$$
$$\mu = 1 - m/M . \qquad (2)$$

For $\zeta > 2$, these equations can be combined to give

$$\rho/\rho_o \approx \mu . \qquad (3)$$

The quantity μ has the value one at the ablation surface and zero at infinity. It represents the fractional thickness of the blowoff from the outside in, to a mass distance m from the ablation surface. Studies of ion rarefaction waves in plane geometry have given similar expressions for the density profile.[2,3]

The degree of ionization Z of the blowoff is obtained from an approximate solution of the Saha equation using the approach by Zel'dovich and Raizer,[4] which assumes the ionization levels I_z are a continuous, rather than discrete function of Z:

$$Z = [2/n_o][2\pi m_e kT/h^2]^{3/2} \exp(-I_z/kT) ,$$
$$n_o = \rho_o N_o/A , \quad n_\infty = Z n_o . \qquad (4)$$

For simplicity, the ionization value used throughout the blowoff is calculated using the density at the ablation surface. Ionization levels calculated by Cowan[5] are available for use in this equation. Using Kramer's formula corrected for induced emissions for the inverse bremsstrahlung cross section, expressed in units of area per unit mass,

$$\kappa_o^L = [4/3][2\pi/[3kT]]^{1/2}[N_o/A]^2$$
$$[\rho Z^3 e^6/[hcm_e^{3/2}\nu^3]][1 - \exp(-h\nu/[kT])] ,$$
$$\kappa^L(\mu) = \mu \kappa_o^L , \qquad (5)$$

expressions (derived in the next section of this paper) are obtained for the location μ_L of peak laser absorption in the blowoff

$$\mu_L = [\kappa_o^L M]^{-1/2} \text{ for } [\kappa_o^L M]^{-1/2} \le 1 ,$$
$$= 1 \qquad \text{for } [\kappa_o^L M]^{-1/2} > 1 , \qquad (6)$$

the linear distance of the laser absorption plane, z_L, from the ablation surface (using Eqs. 2, 3, and 6)

$$z_L \approx v\, t[\pi/4][\ell n \mu_L^{-1}]^{1/2} , \qquad (7)$$

and the fraction ε_L of laser penetration to the ablation surface

$$\varepsilon_L = [1 - \exp(-\ell_M^L)]/\ell_M^L , \quad \ell_M^L = 0.5\, M\, \kappa_o^L . \qquad (8)$$

The quantity ℓ_M^L is the thickness of the blowoff to the laser photons expressed in number of mean free paths.

Similarly, the location μ_c (or z_c) of the critical surface is

$$\mu_c = \rho_c/\rho_o = n_c n_\infty \text{ for } n_\infty/n_\infty \le 1 , \; n_c = \pi m_e c^2/(e^2\lambda^2) ,$$
$$= 1 \qquad \text{for } n_\infty/n_\infty > 1 .$$
$$z_c = v\, t[\pi/4][\ell n \mu_c^{-1}]^{1/2} . \qquad (9)$$

For the region of interest here, calculations with this model indicate that nearly all laser photons are absorbed by inverse bremsstrahlung before reaching the critical surface. Kramer's formula for the inverse bremsstrahlung cross section breaks down when the degree of ionization Z becomes small and gives values less than the real cross section. The model ignores the Gaunt factor (i.e., assumes it to be 1) in the inverse bremsstrahlung cross section for the following reasons: the factor is normally about 1, except near the critical surface; the critical surface is treated separately and does not normally exist in the blowoff anyway; inclusion of the Gaunt factor interferes with scaling of the absorption coefficient with density.

Figure 3 of Ref. 1 presents the Rosseland mean opacity from the SESAME Equation of State Library[3] for aluminum as a function of temperature and density. Examination of this figure shows that the Rosseland mean opacity κ_{Al}^R for aluminum over the range of temperatures and densities of interest to this work can be approximated by

$$\kappa_{Al}^R(m^2/kg) = 6 \times 10^4\, T(eV)^{-2}\, \rho(kg/m^3) ,$$
$$\kappa^R(\mu) = \mu \kappa_o^R , \qquad (10)$$

As in the case of the inverse bremsstrahlung absorption coefficient, this Rosseland mean opacity for the thermal radiation is approximately proportional to ρ so that the opacity at position μ is approximately μ times κ_o^R, the Rosseland mean opacity at the ablation surface. In some regions, values from Eq. 10 differ significantly from the

tables; for more accurate modeling in a particular region of interest, a relation normalized to the tables in that region would be more appropriate.

Assuming that the location of peak laser absorption is the principal source region for thermal radiation in the blowoff, and using Eq. 10 for the Rosseland mean opacity, expressions are obtained for the fraction ε_i (i implies "in") of thermal radiation reaching the ablation surface

$$\varepsilon_i = [1 - \exp(-\ell_L^R)]/\ell_L^R , \quad \ell_L^R = \ell_M^R[1 - \mu_L^2] ,$$

$$\ell_M^R = 0.5\, M\, \kappa_o^R , \tag{11}$$

and for the fraction ε_o (o implies "out") lost into the vacuum

$$\varepsilon_o = [1 - \exp(-\ell_{Lo}^R)]/\ell_{Lo}^R , \quad \ell_{Lo}^R = \ell_M^R\, \mu^2 . \tag{12}$$

Using the above expressions, two flux balance equations based upon conservation of energy are assumed to hold. These two equations are integrated over time to yield energy balance equations; one is an overall energy balance; the other is an energy balance at the ablation surface. Energy transport by monochromatic laser radiation and by thermal radiation are considered; electron conduction in the blowoff is ignored. Conduction in the blowoff does not appear to be significant in the region of interest in this paper. Attentuation of both the laser and thermal radiation by the blowoff is included.

The overall balance equates the laser energy absorbed to the energy absorbed by the target F_s plus the energy radiated into the vacuum

$$\alpha F_o = F_s + \varepsilon_o \sigma T^4 \tau . \tag{13}$$

The energy absorbed by the target is assumed to equal the energy conducted into the solid, the energy to vaporize and ionize the blowoff, plus the thermal kinetic energy of the blowoff

$$F_s = [(4/\pi)K c_p \rho \tau]^{1/2}\, T_s + M[\Delta H + (N_o/A)\Sigma I_z + (3/2)N_o kT/\bar{A}] . \tag{14}$$

Translational kinetic energy of the blowoff and radiation energy within the blowoff are ignored. The balance at the ablation surface equates the energy reaching the ablation surface with that absorbed by the target

$$\varepsilon_i \alpha F_o + \varepsilon_i \sigma T^4 \tau = F_s . \tag{15}$$

All of the above equations are written parametrically in terms of temperature. As discussed below, a self-consistent solution can be found by iteration that determines the blowoff mass and laser fluence absorbed for any given temperature. The laser fluence absorbed αF_o is assumed to be the incident fluence F_o times α, which is one minus the reflectivity. The model does not predict the reflectivity; however, from other sources of information it appears that the reflectivity is near zero when the blowoff is highly ionized, but the reflectivity can be as high as 0.75 for some conditions near the threshold.

The (specific) impulse (momentum per unit area integrated over all time) is obtained by multiplying the blowoff mass M times the average blowoff velocity $\bar{v}$ times a geometric factor G

$$I(\infty) = G\, M\, \bar{v} . \tag{16}$$

The geometric factor is included in the equation for the impulse to account for the directionality of the blowoff; if all blowoff is directed normal to the surface, this factor is equal to 1; if the blowoff is isotropic into 2π solid angle away from the blowoff surface, this factor is equal to 1/2. Experiments generally tend to indicate that this factor is fairly close to 1.

From the density and temperature, the pressure at the ablation surface can be calculated

$$p_o(t \le \tau) = G\, n_o [1 + Z] kT . \tag{17}$$

Because of the assumptions of constant temperature and mass ablation rate, this calculated pressure is constant during the laser pulse. Multiplying this pressure by the pulse length gives an impulse that is equal to 1/2 of the total impulse calculated above using the blowoff mass

$$I(\tau) = [1/2] G\, M\, \bar{v} = p_o \tau . \tag{18}$$

Assuming that the pressure decays exponentially after the laser pulse ends and that the other half of the impulse is imparted during the pressure decay after the pulse, then the time constant for this decay is equal to the laser pulse length, that is

$$p_o(t \ge \tau) = G\, n_o [1 + Z] kT \exp(-[t - \tau]/\tau) . \tag{19}$$

B. Energy Balance

In this section, expressions are developed for the energy flux onto the ablation surface as well as the energy lost back into the vacuum. These expressions are then used in equations for energy balance described in the previous section.

Attenuation of the thermal radiation is estimated by finding the location of peak energy deposition of the laser photons and assuming this is a hot plane in the blowoff cloud (as a perturbation to the assumption of constant temperature in the blowoff). The hot plane is assumed to radiate a flux of σT^4, both inward and outward. Assumed emission from this single plane is reasonable because of the strong T^4 factor. The assumed emission rate (σT^4) is an upper limit and the actual rate could be substantially smaller in some circumstances, for example, if this region were optically thin to the thermal radiation. It is not clear how an error of this nature would affect the impulse because there are compensating factors; more emission increases the mass loss and the impulse, but it also increases energy loss into the vacuum, which decreases the

impulse. Given the emission plane, attenuation of the thermal radiation is obtained using an approximate expression for the Rosseland mean opacity.

The location of the peak laser absorption is obtained by considering both the inverse bremsstrahlung cross section and the critical surface. In some cases, the energy density does not reach a maximum in the blowoff, in which case the hot plane is taken to be the ablation surface. If the critical surface is located on the laser side of the calculated location of peak laser deposition based upon inverse bremsstrahlung, then the hot plane is taken to be the critical surface because the laser photons can not penetrate beyond the critical surface. This only happens early in the pulse, if at all, under the assumption of constant ablation rate for the region of parameter space of interest in this work.

A photon flux φ is attenuated by a mass (per unit area) increment dm with cross section κ (area per unit mass) by an amount specified by

$$d\varphi/\varphi = -\kappa\, dm \quad . \tag{20}$$

Integrating this equation over the blowoff into the position μ gives the flux at position μ as

$$\varphi(\mu) = \alpha\, \varphi_o \exp(-\ell_M^b \mu^2) \quad , \tag{21}$$

where $\alpha\varphi_o$ is the laser flux incident on the target corrected for reflection (α equals one minus the reflectivity). The energy density $\xi(\mu)$ (per unit mass) can be found by taking the derivative of Eq. 21 with respect to mass depth m giving

$$\xi(\mu) = \kappa_o^b\, \mu\, \varphi(\mu) \quad . \tag{22}$$

Taking the derivative of Eq. 22 with respect to mass and setting it equal to zero and solving for μ ($= \mu_L$; L $\Rightarrow$ laser absorption plane) gives the location of the maximum energy density as given above in Eq. 6. For constant ablation rate ($\dot{M} = M/\tau$), the condition on Eq. 6 implies that the peak energy density is at the ablation surface for a time t_o given by

$$t_o = [\kappa_o^b \dot{M}]^{-1} \quad . \tag{23}$$

When the free electron density for the blowoff at the ablation surface n_∞ is greater than the critical electron density n_{ec}, then there a critical surface in the blowoff where this ratio of electron densities equals one. Since the model assumes that Z is constant in the blowoff, the location of the critical surface μ_c is obtained by setting this ratio equal to the mass density ratio as in Eq. 9.

Assuming constant ablation rate, Eqs. 6 and 9 show that μ_i has a fixed value independent of time but that μ_L decreases with time because M is proportional to time ($M = [\dot{M}]\, t$ for $t \le \tau$). Also, at the beginning of the pulse, μ_L always equals 1 (i.e., the maximum energy density, calculated upon the basis of inverse bremsstrahlung, is at the ablation surface) because at the beginning of the pulse, M equals zero. The value μ_c depends on rates alone while μ_L also depends on the integrated mass ablated. Thus, if there is a critical surface in the blowoff, the laser photons encounter it at early time before reaching the plane of maximum energy density by inverse bremsstrahlung absorption. However, if the pulse lasts long enough and constant ablation rate is maintained (by some secondary energy transfer process), then the peak energy density plane will eventually cross the critical surface, preventing most of the remaining incident laser photons from reaching the critical surface. The time t_c at which the crossing occurs can be found by setting $\mu_c = \mu_L$ giving

$$t_c = t_o/\mu_i^2 \quad . \tag{24}$$

Using Eq. 10 in integrating Eq. 20 from the hot plane at μ_L inward to where $\mu_L = 1$ gives the thermal radiated flux emitted onto the ablation surface as

$$\sigma T^4 \exp(-\ell_M^R[1 - \mu_L^2]) \quad . \tag{25}$$

Similarly, the thermal radiated flux emitted outward from the hot plane at μ_L is given by

$$\sigma T^4 \exp(-\ell_M^R \mu_L^2) \quad . \tag{26}$$

Looking from the hot plane inward, the density increases with distance from the hot plane and the blowoff in this region is likely to be optically thick which means that use of the Rosseland mean opacity should be a reasonable approach. However, looking outward, the density decreases and the blowoff in this region would be more likely optically thin. Thus, in some cases, the Planck mean opacity might be a better approximation for use in Eq. 26.

The total flux balance for the blowoff is given in Eq. 18 of Ref. 1 but does not include attenuation of the thermal radiation. Adding this attenuation, as in Eq. 26 above, the total flux balance becomes

$$\alpha\varphi_o = \varphi_i + \sigma T^4 \exp(-\ell_M^R \mu_L^2) \quad . \tag{27}$$

The new equation, added to the model developed in Ref. 1, is the flux balance at the ablation surface. It is based upon the assumption that a local energy balance must occur at all times, which basically determines the ablation rate—a very important quantity. That is, the rate of energy flow to the surface from the laser plus that from thermal radiation is set equal to the rate of energy conduction into the target plus the rate of energy consumption to make the transition to the ionized state. No attempt is made at modeling this ablation region in detail; in particular, it is assumed that the temperature of the material jumps from that of the solid (or liquid, not distinguishing which) to that of the ionized blowoff. However, the energy to make this jump should be important and is therefore accounted for with relative accuracy. Combining these assumptions gives the following equation for this energy balance:

$$\alpha\varphi_o \exp(-\ell_M^R \mu_L^2) = \sigma T^4 \exp(-\ell_M^R[1 - \mu_L^2]) = \varphi_i \tag{28}$$

where

$$\varphi_a = [(2/\pi)Kc_p\rho/\tau]^{1/2} T_e + [\dot{M}][\Delta H + (N_o/A)\Sigma I_z + (3/2)N_o kT/\bar{A}] \quad (29)$$

The quantity φ_a is the flux of energy absorbed by the target. In Eqs. 27 and 28, μ_L is a function of time. As indicated above, it should be possible to solve these equations along with the supporting equations above to find M, and the other parameters of interest, as a function of time. However, in the interest of simplicity, these can be integrated over time if the mass ablation rate and the flux are assumed to be simple functions of time. Assuming these quantities are constant and integrating Eqs. 27 and 28 over time gives the energy balance presented in Eqs. 13, 14 and 15. In these equations ε_L, ε_i, and ε_o are respectively the attenuation factors for: the laser photons onto the ablation surface, the thermal radiation from the hot plane in to the ablation surface, and the thermal radiation from the hot plane out of the blowoff. The laser attenuation factor ε_L is given by Eq. 8 and results directly from integration of Eq. 28.

In Eq. 6 for μ_L the value of $M = M(t) = [\dot{M}]\,t$ varies during the pulse from 0 to $M(\tau)$. Equations 20 and 28 can be integrated using this time dependence for M; however, in the interest of simplicity, equations are given here for ε_i and ε_o for the case where μ_L has a constant value given by Eq. 6 with M replaced by its mean value, 0.5 M. This gives relations for ε_i and ε_o given in Eqs. 11 and 12.

C. Solution of Equations

The equations for the model are summarized in the Appendix B. These coupled equations are expressed parametrically in terms of T. A consistent solution can be found by iterating on the ionization Z and the blowoff mass M. For example, for a given set of inputs (for some temperature T), two guesses each for Z and M can be selected. Then φ and ρ can be calculated, which facilitates an iterative solution for Z. Next, the attenuations (ε) can be calculated, followed by evaluation of the two equations for F_o, which will not agree unless the appropriate value for M is used. Finally, the whole procedure can be iterated on M until the appropriate value of M is found. This has been programmed on an HP-41CVX hand calculator. A consistent solution typically takes a few minutes on the calculator, depending on the accuracy of the guesses.

III. CALCULATIONS WITH THE MODEL

Results from the model for KrF and CO_2 lasers incident on aluminum, with pulse lengths from 10^{-9} to 10^{-3} s at fluences from the impulse threshold up to over 10^{10} J/m^2 (10^6 J/cm^2) are plotted in Figs. 1-3. The ratio of impulse to fluence (impulse coupling coefficient) as a function of fluence is plotted in Fig. 1. The same ratio is replotted versus flux in Fig. 2. In Fig. 3, part of these results are replotted versus fluence to allow direct comparison of the

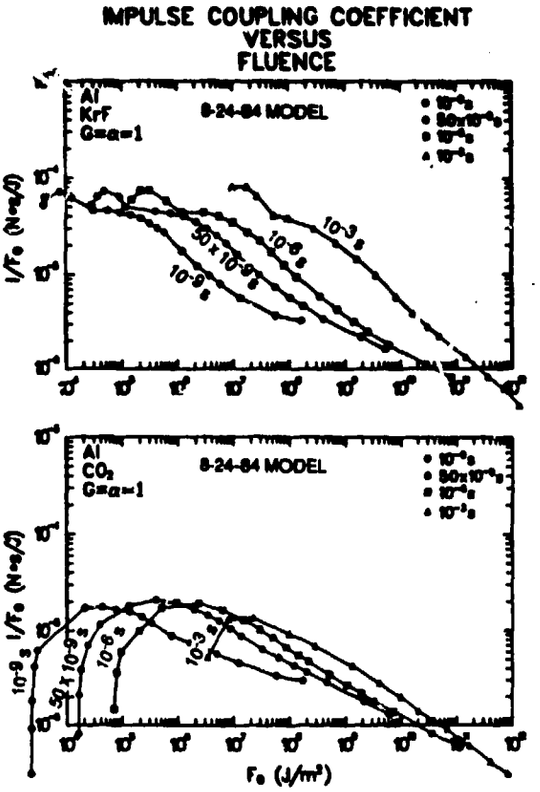

Figure 1. Impulse coupling coefficients versus fluence calculated with the present model (developed on 8-24-84) for CO_2 and KrF lasers with pulse widths of 10^{-9}, 50×10^{-9}, 10^{-6}, and 10^{-3} s normally incident on flat aluminum targets in a vacuum. These calculations were done with $G = \alpha = 1$.

coupling for KrF and CO_2 lasers for different pulse lengths. These results show a threshold, a maximum coupling, and a decrease in coupling at high fluence. The mass loss would have to increase in proportion to the fluence to avoid this decrease. If after some point, there was no increase in mass loss, then the coupling would decrease as the square root of fluence provided the radiation loss into vacuum did not increase with fluence. However, under these conditions radiation losses should increase with fluence causing the coupling to decrease even faster. In some cases, the figures show the coupling decreases about as the square root of fluence (e.g., KrF, 10^{-6} s); this results from some increase in mass loss with fluence as well as some increase in radiation loss with fluence. Figures 1 and 2 show that the order of the curves for different pulsewidths reverses when the absessa is switched from fluence to flux (the flux is the fluence divided by the pulse width); in either case, the coupling depends on pulse width. Interesting, if the coupling coefficients are plotted as a function of fluence divided by the square root of the pulse width, then the results from this model for different pulse widths nearly merge into one curve, especially for the KrF laser. Figure 3 shows that at very high fluences and fluxes the model predicts that the coupling coefficient curves for KrF and CO_2 merge; this is because the plasma is becoming very opaque to photons of

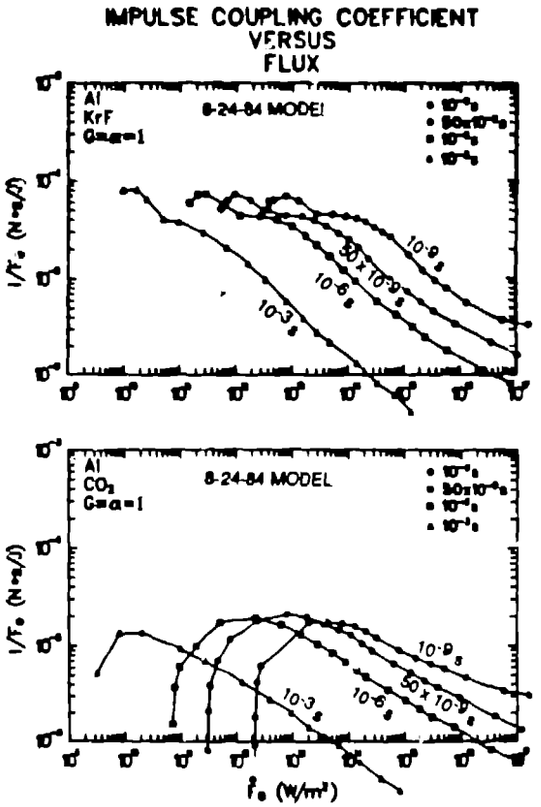

Figure 2. Impulse coupling coefficients versus flux calculated with the present model for CO_2 and KrF lasers with pulse widths of 10^{-9}, 50×10^{-9}, 10^{-6}, and 10^{-3} s normally incident on flat aluminum targets in a vacuum. These calculations were done with $G = \alpha = 1$.

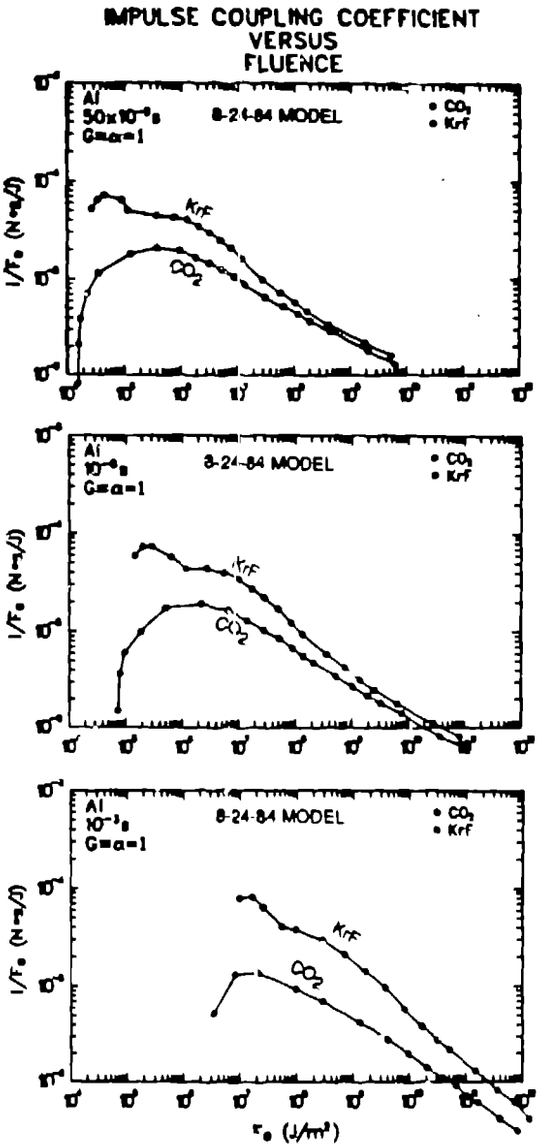

Figure 3. Impulse coupling coefficients versus fluence calculated with the present model for CO_2 and KrF lasers with pulse widths of 50×10^{-9}, 10^{-6}, and 10^{-3} s normally incident on flat aluminum targets in a vacuum. These calculations were done with $G = \alpha = 1$.

both laser wavelengths in this region (so that most of the mass ablation is by secondary energy transfer) making the impulse independent of the laser. When the flux becomes too large, the model becomes invalid because of additional phenomena not included.

Results from the model for aluminum targets, using $G = \alpha = 1$, are compared with both experimental measurements[7,8,9] and LASNEX computer calculations[10,11] in Figs. 4-6. Figure 4 is for a CO_2 laser (Gemini) with about a 2-ns pulse width. The Gemini data are for titanium and various other targets (including organics but not aluminum).[7] Since the data show that the coupling is almost material-independent it seems appropriate to compare the data with model calculations for aluminum, and in fact, Fig. 4 shows good agreement between the model and the data. Figure 5 is for the same CO_2 laser (Gemini) modified to have about a 2-μs pulse length.[8] The comparison with aluminum is within about a factor of 2. LASNEX calculations for Al at high fluence are included in Fig. 5. These values are a factor of 2 to 3 lower than values from the model. The experimental data, which only exist at a fluence up to the lowest LASNEX fluence, are between the model and LASNEX results.

Figure 6 is for 50 ns, KrF laser exposure of aluminum.[9] The agreement between the model (with $\alpha = 1$) and the experimental data are reasonably good in the region of 10^4 to 10^7 J/m^2. At lower fluence, a substantial fraction of the incident photons are probably reflected, causing the values calculated with the model with $\alpha = 1$ to give a coupling that is too large. Using a smaller value of α would improve agreement with experiment and reflectives are known to be sizable in this region. At fluences above 10^7 J/m^2, the experimental data is 2-dimensional because of the small spot size; in this region the measured coupling agrees reasonably well with the 2-D LASNEX runs but is considerably larger than that calculated by either the model or 1-D LASNEX runs.

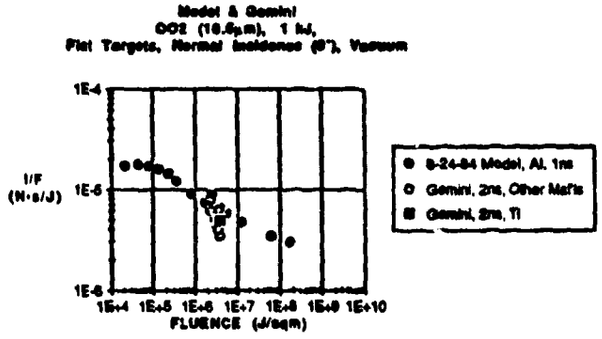

Figure 4. Comparison of calculations using the present model (using $G = \alpha = 1$) with data from a CO_2 laser with pulse width of about 2 ns normally incident on flat targets in a vacuum.

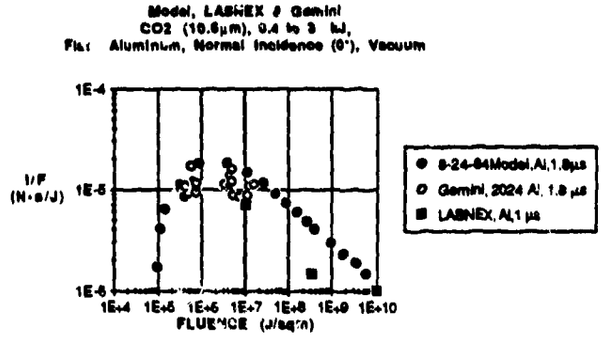

Figure 5. Comparison of calculations using the present model (using $G = \alpha = 1$), with LASNEX calculations, and with data from a CO_2 laser with pulse width of about 2 μs normally incident on flat targets in a vacuum.

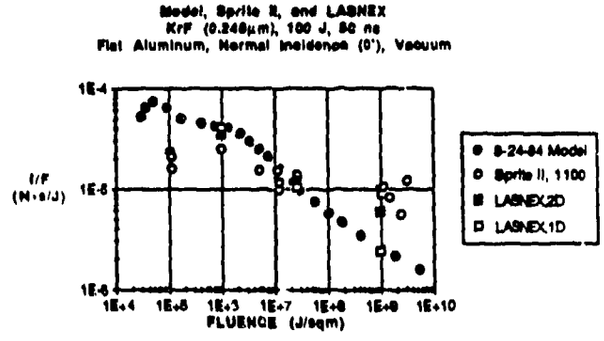

Figure 6. Comparison of calculations using the present model (using $G = \alpha = 1$), with LASNEX calculations, and with data from a KrF Laser with an energy of about 100 J and a pulse width of about 50 ns normally incident on flat aluminum targets in a vacuum.

REFERENCES

1. R. S. Dingus, "Phenomenology of Optical-Laser-Induced Impulse in Vacuo," Los Alamos National Laboratory internal document SDR/U:84-92 (March 8, 1984), to become document LA-10113.

2. J. E. Allen and J. G. Andrews, "A Note on ION Rarefaction Waves," *J. Plasma Physics*, 4, 187-194 (1970).

3. J. E. Crow, P. L. Auer, and J. E. Allen, "The Expansion of a Plasma into a Vacuum," *J. Plasma Physics*, 14, part 1, 65-76 (1975).

4. Y. Zel'dovich and Y. Razier, *Physics of Shock Waves and High-Temperature Hydrodynamic Phenomena*, (Academic Press, New York and London, 1966).

5. R. D. Cowan, *The Theory of Atomic Structure and Spectra* (University of California Press, Berkeley, 1981).

6. "SESAME '83: Report on the Los Alamos Equation-of-State Library," Los Alamos National Laboratory document LALP-83-4 (February 1983).

7. R. S. Dingus and D. M. Barrus, "Pulsed Laser Effects—Measurements with the Gemini Laser," Presentation to Directed Energy Effects and Vulneability Workshop (June 1982).

8. W. Z. Osborne, T. R. King, C. R. Phipps, Jr., R. J. Scammon, and D. M. Barrus, "Single-Pulse Laser Effects Measurements at 2.8 and 10.6 μm," published in these proceedings.

9. R. S. Dingus, T. R. King, W. Z. Osborne and C. R. Phipps, Jr., "Single-Pulse Laser Effects Measurements at 248 nm", AIAA paper in these proceedings of Laser Effects Conf.

10. S. R. Goldman, G. H. Canavan, R. S. Dingus, and M. A. Mahaffy, "Simulation of the Interaction of Single-Pulsed Optical Lasers with Targets in a Vacuum," in A. S. Kaye and A. C. Walker, (Eds.), *Gas Flow and Chemical Lasers*, 1984 (Adam Hilger, Bristol, 1985), p. 125.

11. S. R. Goldman, J. S. Saltzman, and R. S. Dingus, "Simulation of Laser-Target Interactions in a Vacuum," published in these proceedings.

APPENDIX A

GLOSSARY

Material Properties of target

- A = Atomic Mass
- K = Thermal conductivity
- c_p = Specific heat
- ρ_s = solid density
- T_s = sublimation temperature
- ΔH = sublimation energy (enthalpy)
- I_z = Ionization energy levels
- $\bar{I}_z$ = "continuous ionization function"

Laser Properties

- α = Absorptivity = 1 − Reflectivity = Fraction of laser photons absorbed
- τ = Pulse width
- $h\nu$ = Photon energy
- φ_o = Incident Flux (intensity)
- F_o = Incident Fluence

Other Values

- I = Impulse = momentum per unit area
- T = Temperature of blowoff
- G = Geometric factor
- p_o = pressure at ablation surface
- z = linear distance from ablation surface
- δ = thermal diffusion distance in target
- ρ = $\rho(z)$ = density (mass per unit volume) of blowoff at position z
- ρ_o = density of blowoff at ablation surface
- N_o = Avogadro's Number
- k = Boltzmann Constant
- γ = ratio of specific heats
- n_o = $\rho_o N_o/A$ = Number of atoms per unit volume in blowoff at ablation surface
- Z = Number of free electrons per atom
- n_{eo} = Zn_o = Number of free electrons per unit vol in blowoff at ablation surface
- n_{ec} = Number of free electrons per unit vol at critical surface
- $\bar{A}$ = $A/[1 + Z]$ = average atomic mass per free particle
- $\bar{v}$ = Average particle velocity for Maxwell-Boltzmann distribution
- z_o = $\bar{v}\,\tau$ = average distance particles move during laser pulse
- ζ = $[4/\pi][z/z_o]$ = scale distance from ablation surface
- m = $m(z) = \int_0^z \rho(z')dz'$ = mass (per unit area) depth in blowoff
- $\dot{M}$ = mass ablation rate
- M = $M(t) = m(z = \infty)$ at time t
- M_t = $M(\tau)$ = total mass ablated
- μ = $1 - m/M$ = fractional mass thickness of blowoff from outside in to m
- μ_L = location of peak laser absorption in terms of μ
- z_L = linear position of peak laser absorption
- μ_c = location of critical surface in terms of μ
- z_c = linear position of peak laser absorption
- κ^L = $\kappa^L(\mu)$ = (inverse brem.) absorption coefficient for laser photons at μ
- ℓ_M^L = mean free path of blowoff to laser photons
- ε_L = attenuation at ablation surface of laser photons by blowoff
- σ = Stefan-Boltzmann constant
- κ^R = $\kappa^R(\mu)$ = thermal radiation opacity at μ
- κ_o^R = thermal radiation opacity at ablation surface
- ℓ_M^R = thermal radiation mean free path of blowoff
- $\ell_{L_i}^R$ = thermal radiation mean free path in from μ_L to ablation surface
- ε_i = attenuation of thermal radiation in from μ_L to ablation surface
- $\ell_{L_o}^R$ = thermal radiation mean free path out from μ_L to vacuum
- ε_o = attenuation of thermal radiation out from μ_L to vacuum
- $\xi(\mu)$ = energy density at μ from laser deposition
- t_o = time at which peak energy density leaves ablation surface
- t_c = time at which peak energy density crosses critical surface
- e = charge of electron
- m_e = mass of electron
- h = Planck constant
- c = speed of light
- ν = frequency of laser photons
- λ = wavelength of laser photons

APPENDIX B

MODEL

Input $T, G, \alpha, \tau, h\nu, A, K, c_p, \rho_s, T_s, \Delta H, I_z$

Assume: $\varphi_o = \text{const.} = F_s/\tau$ for $t \le \tau$; $\dot{M} = \text{const.} = M_s/\tau$ for $\tau \le \tau$
$= 0$ for $t > \tau$ $= 0$ for $t > \tau$

Coupled Equations expressed parametrically in terms of T:

$$I(\tau) = [1/2]G\,M\,\mathring{v} = p_o\,\tau\,, \qquad p_o = G\,n_o[1 + Z]kT \quad \text{for } t \le \tau\,,$$
$$I(\infty) = G\,M\,\mathring{v} = G\,n_o[1 + Z]kT\exp(-[t - \tau]/\tau) \quad \text{for } t \ge \tau\,,$$

$$\mathring{v} = \{[8/\pi]N_o kT/\tilde{A}\}^{1/2}\ \tilde{A} = A/(1 + Z)\,,$$

$$Z = [2/n_o][2\pi m_e kT/h^2]^{3/2}\exp(-I_z/kT)\,, \quad n_o = \rho_o N_o/A\,, \quad n_\infty = Z\,n_o$$

$$z_o \equiv \mathring{v}\,\tau\,, \quad \zeta \equiv [4/\pi][z/z_o]\,, \quad \rho/\rho_o = \exp(-\zeta^2) \approx 1 - m/M \equiv \mu\,, \quad \rho_o = [4/\pi]\dot{M}/\mathring{v}\,, \quad m/M = \text{erf}(\zeta)$$

$$\alpha F_o = F_s + \varepsilon_o\sigma T^4\tau\,, \quad \varepsilon_L\alpha F_o + \varepsilon_i\sigma T^4\tau = F_s$$

$$F_s = [\{4/\pi\}Kc_p\rho\tau]^{1/2}\,T_s + M[\Delta H + \{N_o/A\}\,\Sigma\,I_z + \{3/2\}N_o kT/\tilde{A}]$$

$$\delta\rho_s = [4K\rho_s\tau/c_p]^{1/2}\,, \qquad \gamma - 1 = kT/[\{3/2\}kT + [\Sigma\,I_z]/[1 + Z]]\,,$$

$$(I/F_o)_{max} \le 2\,\alpha\,G/[3\pi\Delta H]^{1/2} \text{ at } \alpha F_o = 2\,M\,\Delta H$$

$$\kappa_o^L = [4/3]\{2\pi/[3kT]\}^{1/2}[N_o/A]^2\{\rho Z^3e^6/[hcm_e^{3/2}\nu^3]\}\{1 - \exp(-h\nu/[kT])\}\,, \quad \kappa^L(\mu) = \mu\,\kappa_o^L$$

$$\kappa_{o,AS}^R(m^2/kg) = 6 \times 10^4\,T(eV)^{-2}\,\rho(kg/m^3) \qquad \kappa^R(\mu) = \mu\,\kappa_o^R$$

$$\mu_L = [\kappa_o^L M]^{-1/2} \text{ for } [\kappa_o^L M]^{-1/2} \le 1\,, \quad \mu_c = \rho_c/\rho_o = n_{oc}/n_{oo} \text{ for } n_{oc}/n_{oo} \le 1$$
$$= 1 \text{ for } [\kappa_o^L M]^{-1/2} > 1\,, \quad = 1 \text{ for } n_{oc}/n_{oo} > 1$$

$$t_o = [\kappa_o^L\dot{M}]^{-1}\,, \qquad t_c = t_o/\mu_c^2\,, \qquad n_{oc} = \pi m_e c^2/(e^2\lambda^2)$$

$$z_L = \mathring{v}\,t[\pi/4][\ell n\mu_L^{-1}]^{1/2}\,, \qquad z_c = \mathring{v}\,t[\pi/4][\ell n\mu_c^{-1}]^{1/2}$$

$$\ell_M^L = 0.5\,M\,\kappa_o^L\,,$$

$$\ell_M^R = 0.5\,M\,\kappa_o^R\,, \qquad \ell_L^R = \ell_M^R[1 - \mu_L^2]\,, \qquad \ell_{Lo}^R = \ell_M^R\,\mu^2\,,$$

$$\varepsilon_L = [1 - \exp(-\ell_M^L)]/\ell_M^L\,, \quad \varepsilon_i = [1 - \exp(-\ell_L^R)]/\ell_L^R\,, \quad \varepsilon_o = [1 - \exp(-\ell_{Lo}^R)]/\ell_{Lo}^R$$